Numerical modeling of collisional dynamics of Sr in an optical dipole trap

M. Yan, R. Chakraborty, A. Mazurenko, P. G. Mickelson, Y. N. Martinez de Escobar, B. J. DeSalvo, and T. C. Killian

Phys. Rev. A **83**, 032705 — Published 9 March 2011

DOI: 10.1103/PhysRevA.83.032705

Numerical modeling of collisional dynamics of Sr in an optical dipole trap

M. Yan, R. Chakraborty, A. Mazurenko, P. G. Mickelson, Y. N. Martinez de Escobar, B. J. DeSalvo, and T. C. Killian
Rice University, Department of Physics and Astronomy, Houston, Texas, 77251

We describe a model of inelastic and elastic collisional dynamics of atoms in an optical dipole trap that utilizes numerical evaluation of statistical mechanical quantities and numerical solution of equations for the evolution of number and temperature of trapped atoms. It can be used for traps that possess little spatial symmetry and when the ratio of trap depth to sample temperature is relatively small. We compare simulation results with experiments on ^{88}Sr and ^{84}Sr, which have well-characterized collisional properties.

PACS numbers:

I. INTRODUCTION

Understanding the collisional dynamics of trapped, ultracold atoms is essential for optimizing forced evaporative cooling [1, 2] and obtaining quantum degenerate Bose [3] and Fermi gases [4]. It also allows determination of ultracold collision properties from the evolution of number and temperature in a trapped sample of atoms or molecules [5–7].

Many recipes have been presented for relating the evolution of the trapped gas to underlying physical parameters. Typically the collisional dynamics are described by differential equations for the time rate of change of the atom number (N) and and total energy (E), as originally suggested by [1, 2]. The method has been extended and developed in many other works [8–15]. The standard treatment of evaporation is described by Luiten *et al.* [10], which derives expressions for thermodynamic quantities from the kinetic equations using an assumption of sufficient ergodicity and a truncated Boltzmann velocity distribution. Analytic evaluation of these expressions is straightforward for power-law traps. Noteworthy subsequent improvements over this work include the addition of effects of time-dependent potentials [11], energy-dependent cross sections [12], and quantum statistics [13]. Prescriptions have been offered for optimizing evaporation [14] and deriving scaling laws [15]. Direct Monte Carlo simulations have also been presented to relax the assumption of sufficient ergodicity [16] and treat hydrodynamic effects [17].

A common simplifying assumption is that η, the ratio of trap depth ϵ_t to sample temperature $k_B T$ is large, where k_B is the Boltzmann constant. For example, this yields analytic expressions for thermodynamic quantities, and allows approximation of optical dipole traps [18] as parabolic potentials [19]. By taking advantage of the high degree of spatial symmetry in a linear potential, analytic expressions for thermodynamic quantities were derived for the low-η situation ($\eta < 4$) in this particular geometry [20]. It is worth emphasizing that Luiten's model [10] is, in principle, valid for low η as long as the assumptions of ergodicity and a truncated Boltzmann distribution are also valid.

If the potential lacks the ideal shape of a power-law trap, simple analytic expressions for many quantities of interest cannot be found, and numerical methods are required. This is the case for low η in an optical dipole trap and especially when gravity is significant. ^{88}Sr in an optical dipole trap falls into this situation because of its large mass and extremely small s-wave scattering length $a_{88} = -1.4(6)\, a_0$ [21], where the Bohr radius $a_0 \approx 0.53$ Å. Here, we describe numerical methods appropriate for modeling collisional dynamics in an arbitrary trap in the low or high η regime, which can be used for ^{88}Sr. Our approach builds on the works of Luiten *et al.* [10] and Comparat *et al.* [19]. As a check of the model, we also compare predictions with measurements of forced evaporation in ^{84}Sr, which has an s-wave scattering length of $a_{84} = 122.7(3)\, a_0$ [21] and attains a much higher η, which allows direct evaporation to quantum degeneracy [22, 23]. This model has also been used to interpret data on collisions involving Sr atoms in metastable states [24] and evaporative cooling of ^{87}Sr and ^{88}Sr for quantum degeneracy studies [25, 26]. The main assumptions are ergodicity and the appropriateness of truncated Boltzmann distributions.

This paper is organized as follows. Section II describes the experimental setup, and then section III presents the collisional processes important in the trapped sample and the differential equations for evolution of N and E. The numerical calculation is described in section IV, and applications of the model to describe trapped ^{88}Sr and ^{84}Sr, are discussed in section V. The appendix describes an approximate treatment of the energy dependence of the ^{88}Sr elastic collision cross section.

II. EXPERIMENTAL SETUP

The creation of samples of ^{88}Sr or ^{84}Sr atoms in an optical dipole trap (ODT) starts with laser cooling and trapping phases that have been described in detail previously [22, 27–29]. Atoms are trapped in a magneto-optical trap (MOT) operating on the 461 nm $^1S_0$-$^1P_1$ transition (Fig. 1) and cooled to about 2 mK. There is a decay channel from the

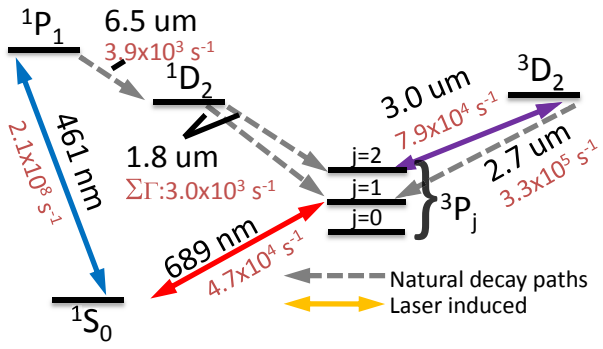

FIG. 1: (Color online) Atomic Sr energy levels involved in laser-cooling. Decay rates (s^{-1}) and excitation wavelengths are given for selected transitions. Laser light used for the experiment is indicated by solid lines. Atoms decaying to the $^3P_2$ level may be repumped by 3 μm light.

$^1P_1$ state, to the $^1D_2$ state with a branching ratio of 2×10^{-5}. $^1D_2$ atoms can decay to the $^3P_1$ state, which decays to the ground state to allow further cooling, or to $^3P_2$ state, which can be trapped and accumulated in the magnetic trap formed by the quadrupole MOT magnets [27]. $^3P_2$ atoms are repumped by applying a 3 μm laser resonant with the $^3P_2$-$^3D_2$ transition that returns these atoms to the ground state [30]. The repumped sample of atoms contains up to 2.5×10^8 ^{88}Sr atoms or 2.5×10^7 ^{84}Sr atoms.

After this initial MOT stage, the 461 nm light is extinguished and the atom sample is transferred with more than 50% efficiency to a second MOT operating on the $^1S_0$-$^3P_1$ intercombination line [31]. The atoms are cooled to 3 μK in the ^{88}Sr sample or 1 μK in the ^{84}Sr sample, both producing peak densities of $\sim 10^{12}$ cm^{-3}.

Atoms are then transferred to an ODT generated from a 21 W, 1064 nm, linearly-polarized, multi-longitudinal-mode fiber laser. The experimental setup is shown in Fig. 2. The trap is in a crossed-beam configuration, derived from the first order deflection of an acousto-optic modulator. The beam is focused on the atoms with a minimum e^{-2} intensity-radius of $w \approx 100\,\mu$m. It is then reflected back through the chamber to intersect the first beam at 90 degrees and refocused to have approximately the same waist at the atoms. Both beams lie in a plane that is inclined 10.5° from horizontal.

The number of atoms and sample temperature are determined with time-of-flight absorption imaging using the $^1S_0$-$^1P_1$ transition. The ODT trapping potential is calculated from measured laser beam parameters and the polarizability of the $^1S_0$ state [32], and it is checked by measuring the trap oscillation frequencies through the parametric resonance technique [33]. This allows us to infer the sample density profile from the temperature and number of trapped atoms.

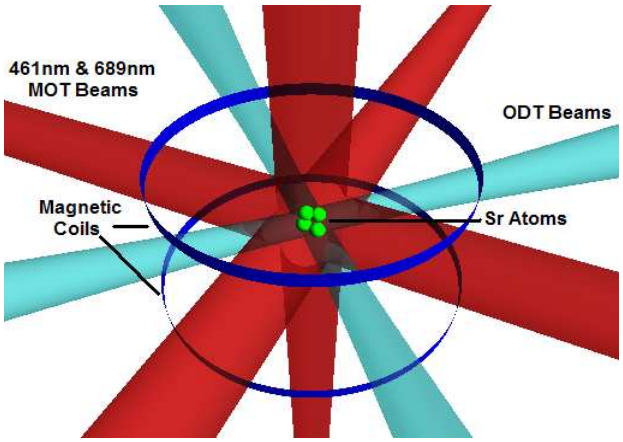

FIG. 2: (Color Online) Schematic of our experiment illustrating the overlap of ODT beams with MOT beams and relative positions of magnetic coils.

III. MODEL OF COLLISIONAL DYNAMICS

The evolution of atom number N and total energy E is described by a system of differential equations. Different terms in the equations represent physical processes such as elastic and inelastic collisions, and processes involving laser fields.

A. Description of Basic Processes

1. Background collisions and inelastic collisional losses

One-body losses due to collisions with background gas, and two- and three-body inelastic collisional losses are described by the local equation

$$\dot{n}_{coll} = -\Gamma_{bg} n - \beta_{in} n^2 - L n^3, \tag{1}$$

where n is the atomic density. In simulations described here, we will assume that the loss rate constants Γ_{bg}, β_{in}, and L are independent of temperature. Integrating Eq. 1 over the trap volume gives

$$\dot{N}_{coll} \;=\; -\left(\Gamma_{bg} + \beta_{in} N \frac{V_2}{V_1^2} + L N^2 \frac{V_3}{V_1^3}\right) N, \tag{2}$$

where the effective volumes are

$$V_q \;\equiv\; \frac{1}{n_{peak}^q} \int d^3 r [n(\mathbf{r})]^q, \tag{3}$$

where n_{peak} is the peak density in the trap. We have also made use of the relationship between peak density and total number, $n_{peak} V_1 = N$.

The energy or temperature evolution due to these processes for a constant trap potential can be found as follows. The rate of energy change in an infinitesimal volume dV is

$$d\dot{E}_{coll} = -\dot{n}_{coll}(\mathbf{r}) dV [U(\mathbf{r}) + \bar{E}_k(\mathbf{r})], \tag{4}$$

where $U(\mathbf{r})$ is the trap potential and $\bar{E}_k(\mathbf{r})$ is the average kinetic energy per atom located at $\mathbf{r}$. $U(\mathbf{r})$ is defined to have a value of $U = 0$ at the trap minimum. We assume a truncated Boltzmann phase-space distribution (this is valid if the trap is sufficiently ergodic [10]), which implies that the kinetic energy in a given differential volume also obeys a truncated Boltzmann distribution truncated at the kinetic energy required for an atom to escape the trap from the differential volume. Thus the position-dependent average kinetic energy can be expressed as

$$\bar{E}_k(\mathbf{r}) = \frac{\int_0^{\epsilon_t - U(\mathbf{r})} dE_k E_k^{3/2} e^{-E_k/k_B T}}{\int_0^{\epsilon_t - U(\mathbf{r})} dE_k E_k^{1/2} e^{-E_k/k_B T}}. \tag{5}$$

Integrating Eq. 4 over the trap volume yields the rate of change of total energy

$$\begin{aligned} \dot{E}_{coll} \;=\; & -\Gamma_{bg}\left(\frac{T_1 + P_1}{V_1}\right) N - \beta_{in}\left(\frac{T_2 + P_2}{V_1^2}\right) N^2 \\ & -L\left(\frac{T_3 + P_3}{V_1^3}\right) N^3. \end{aligned} \tag{6}$$

We have introduced the effective kinetic energies

$$T_q \equiv \frac{1}{n_{peak}^q} \int d^3 r [n(\mathbf{r})]^q \bar{E}_k(\mathbf{r}), \tag{7}$$

and effective potential energies

$$P_q \equiv \frac{1}{n_{peak}^q} \int d^3 r [n(\mathbf{r})]^q U(\mathbf{r}). \tag{8}$$

Note that the total energy of atoms inside the trap is $E = (T_1 + P_1)\frac{N}{V_1}$. To connect with a more intuitive expression, note that in the high-η limit, $\bar{E_k}(\mathbf{r}) = \frac{3}{2}k_BT$, which can be taken out of the integrals to yield

$$\begin{aligned}\dot{E}_{coll}^{high-\eta} &\approx -\frac{3}{2}k_BT\left(\Gamma_{bg}N + \beta_{in}\frac{V_2}{V_1^2}N^2 + L\frac{V_3}{V_1^3}N^3\right) \\ &\quad -\left(\Gamma_{bg}\frac{P_1}{V_1}N + \beta_{in}\frac{P_2}{V_1^2}N^2 + L\frac{P_3}{V_1^3}N^3\right). \end{aligned} \tag{9}$$

2. Off-resonant laser scattering

The scattering of off-resonant photons, such as from the ODT laser, heats the atoms due to momentum diffusion (MD) [34]. The rate of change of total energy due to this process is

$$\dot{E}_{MD} = \Gamma_{laser}NE_{recoil}, \tag{10}$$

where the total scattering rate of light from the laser field is given by Γ_{laser}. If the light scattering rate is dominated by one transition, $\Gamma_{laser} = \frac{s_0\gamma/2}{1+s_0+(2\delta_l/\gamma)^2}$, in which s_0 is the saturation parameter, δ_l is the detuning of the laser, and γ is the linewidth of the transition. The recoil energy is $E_{recoil} = k_BT_{recoil} = \hbar^2k^2/m$, where $\hbar$ is Planck's constant h divided by 2π, k is the photon circular wavenumber, and m is the atom mass.

3. Evaporation

To describe the rate of atom loss due to evaporation, we follow the treatment of [10], which assumes ergodicity and a truncated Boltzmann distribution in phase space,

$$\begin{aligned} f(\mathbf{r},\mathbf{p}) &= \frac{n_0}{(2\pi m k_BT)^{3/2}}\exp\left[-\frac{U(\mathbf{r})+p^2/2m}{k_BT}\right] \\ &\quad \times\Theta(\epsilon_t - U(\mathbf{r}) - p^2/2m). \end{aligned} \tag{11}$$

$\Theta(\epsilon)$ is the Heaviside step function, and $\mathbf{p}$ is the atom momentum with $p = |\mathbf{p}|$. Note that n_0 is not the peak density (the density at the trap minimum) unless the trap is infinitely deep. This yields a density distribution given by

$$\begin{aligned} n(\mathbf{r}) &= n_{peak}Ae^{-U(\mathbf{r})/k_BT}\left\{\mathrm{erf}\left[\sqrt{\frac{\epsilon_t - U(\mathbf{r})}{k_BT}}\right]\right. \\ &\quad \left. -2\sqrt{\frac{\epsilon_t - U(\mathbf{r})}{\pi k_BT}}\exp\left[-\frac{\epsilon_t - U(\mathbf{r})}{k_BT}\right]\right\}, \end{aligned} \tag{12}$$

where the normalization constant A is given by

$$A = \frac{n_0}{n_{peak}} = \left\{\mathrm{erf}\left[\sqrt{\frac{\epsilon_t}{k_BT}}\right] - 2\sqrt{\frac{\epsilon_t}{\pi k_BT}}\exp\left[-\frac{\epsilon_t}{k_BT}\right]\right\}^{-1}. \tag{13}$$

The peak density is given by

$$\begin{aligned} n_{peak} &= n(\mathbf{r})|_{U(\mathbf{r})=0} \\ &= n_0\left\{\mathrm{erf}\left[\sqrt{\epsilon_t/k_BT}\right]\right. \\ &\quad \left. -2\sqrt{\epsilon_t/\pi k_BT}\exp\left[-\epsilon_t/k_BT\right]\right\}. \end{aligned} \tag{14}$$

The total number of atoms lost per unit time due to evaporation can then be written as

$$\dot{N}_{ev} = -\Gamma_{ev}N, \tag{15}$$

where the evaporation rate per atom is

$$\Gamma_{ev} = \frac{N}{V_1^2} A^2 \sigma_{el} \bar{v} e^{-\eta} V_{ev}. \tag{16}$$

Here, σ_{el} is the elastic collision cross section, which is assumed to be collision-energy independent in this treatment. $\bar{v} = \left(\frac{8k_BT}{\pi m}\right)^{1/2}$ is the mean atomic velocity, and the effective volume for elastic collisions leading to evaporation is

$$V_{ev} = \frac{\Lambda^3}{k_BT} \int_0^{\epsilon_t} d\epsilon \rho(\epsilon)[(\epsilon_t - \epsilon - k_BT)e^{-\epsilon/k_BT} + k_BTe^{-\eta}], \tag{17}$$

where

$$\Lambda = (2\pi\hbar^2/mk_BT)^{1/2} \tag{18}$$

is the thermal de Broglie wavelength. The density of states in the trap is given by

$$\rho(\epsilon) = \frac{2\pi(2m)^{3/2}}{h^3} \int_{U(\mathbf{r})\leq\epsilon_t} d^3r \sqrt{\epsilon - U(\mathbf{r})}. \tag{19}$$

Similarly, the rate of change of total energy due to evaporation is

$$\dot{E}_{ev} = -\Gamma_{ev} N \bar{E}_{ev}, \tag{20}$$

where the average energy loss per evaporated atom is

$$\bar{E}_{ev} = \epsilon_t + \frac{V_{ev} - X_{ev}}{V_{ev}} k_BT, \tag{21}$$

with

$$X_{ev} = \frac{\Lambda^3}{k_BT} \int_0^{\epsilon_t} d\epsilon \rho(\epsilon)[k_BTe^{-\epsilon/k_BT} - (\epsilon_t - \epsilon + k_BT)e^{-\eta}]. \tag{22}$$

We note that the assumption of ergodicity that underlies this treatment is equivalent to assuming three-dimensional evaporation, or that any atom with an energy greater than the trap depth escapes the trap before suffering a collision. This assumption is questionable when evaporation is over a saddle point, such as when gravity significantly modifies the potential. However, recent experiments in a similar trap geometry [35] to ours have shown that the evaporation efficiency can be near the three-dimensional limit if the trap is sufficiently asymmetric and non-separable, which is the case here. Hydrodynamic effects can also limit evaporation efficiency when the collisional mean free path is on the order of or smaller than the sample size [19], but our experiments do not approach this regime, and we neglect these effects here.

4. Time- dependent traps : forced evaporation

When the trap confinement is varied adiabatically, such as during forced evaporation in an ODT when the trap-laser intensity is decreased, there is also an energy change due to reduction in the potential energy [11, 15, 19]. This energy change can be expressed as

$$\dot{E}_{pot} = -\Gamma_{pot} N P_1/V_1, \tag{23}$$

where $\Gamma_{pot} = \dot{U}/U$ and P_1/V_1 is the average potential energy per atom. In most experiments with forced evaporative cooling, η is relatively high, and Γ_{pot} can be calculated using a harmonic approximation of the trap. For an isotropic trap, $U(r) = \frac{1}{2}m\omega^2r^2$ and $\Gamma_{pot} = 2\dot{\omega}/\omega$. For a nonisotropic potential, ω is taken as the geometric mean of the angular oscillator frequencies [19]. When describing evaporation of ^{84}Sr in Sec. V, we use this approximation for Γ_{pot}, with P_1, V_1, and ω found numerically for the trap as a function of ODT laser intensity.

5. Final equations

Accounting for all processes, the equations for number and energy evolution become

$$\begin{aligned}\dot{N} &= -\Gamma_{bg}N - \frac{1}{V_1^2}\left(\beta_{in}V_2 + A^2\sigma_{el}\bar{v}e^{-\eta}V_{ev}\right)N^2 \\ &\quad -L\frac{V_3}{V_1^3}N^3, \qquad (24)\\ \dot{E} &= -\Gamma_{bg}\left(\frac{T_1+P_1}{V_1}\right)N - \beta_{in}\left(\frac{T_2+P_2}{V_1^2}\right)N^2 \\ &\quad -L\left(\frac{T_3+P_3}{V_1^3}\right)N^3 + \Gamma_{laser}NE_{recoil} \\ &\quad -\frac{N^2}{V_1^2}A^2\sigma_{el}\bar{v}e^{-\eta}V_{ev}\left[\epsilon_t + \frac{V_{ev}-X_{ev}}{V_{ev}}k_BT\right] \\ &\quad +\frac{2\dot{\omega}}{\omega}\frac{P_1N}{V_1}. \qquad (25)\end{aligned}$$

IV. DESCRIPTION OF THE NUMERICAL PROCEDURE

Equations 24 and 25 and the quantities contained therein provide a complete description of the evolution of the trapped gas within the approximations of ergodicity and a truncated Boltzmann distribution. Approximations are usually made to arrive at analytic results for required quantities (e.g. [19]) in order to facilitate solution of the differential equations. This is straightforward for high-η conditions [9], and also in situations of low-η and with sufficient trap symmetry [20]. For low-η conditions and traps that lack spatial symmetry, numerical evaluation of statistical mechanical quantities is the only option, and that is the approach we follow, with the exception of calculation of Γ_{pot}. Numerical evaluation is essential to describe our experiments with ^{88}Sr in an ODT because of the small scattering rate for this isotope, the importance of gravity, and the small inclination of our trap lasers away from horizontal, which makes the trap very asymmetric. We perform all calculations in $Mathematica^{TM}$.

The first step in the procedure is to find an appropriate expression for the potential, $U(\mathbf{r})$, at a given ODT laser intensity, for input to the numerical calculations. Starting from the theoretical expression for the optical potential [18] created by the known atomic polarizability [32] and laser wavelength, powers, and waists, we employ an algorithm to find the trap minimum, the trap depth (ϵ_t), and the saddle points. This defines the trap boundaries and allows us to offset the trap so that the minimum is $U = 0$. An example is shown in Fig. 3.

The formula for $U(\mathbf{r})$ and description of the boundary is then passed to numerical integration routines for calculating statistical mechanical quantities described in section III at a given temperature. For spatial integrals for V_q (Eq. 3), T_q(Eq. 7), P_q(Eq. 8), and $\rho(\epsilon)$ (Eq. 19), the integration extends over the entire region contained in the trap as determined with the algorithm described above. (This region is the connected region of space with $U(r) < \epsilon_t$ that contains the trap minimum.) An interpolating function representing $\rho(\epsilon)$ is used in evaluation of V_{ev} (Eq. 17) and X_{ev} (Eq. 22) in integrals over an energy interval from 0 to ϵ_t. An adaptive-step-size integration routine in $Mathematica^{TM}$ is used to evaluate these integrals.

To provide a check of our programs, we compared the results of numerical calculations of all statistical mechanical quantities for power-law traps to various analytic expressions that are available in situations with such a simple form of the potential [36]. Expressions in terms of incomplete Gamma functions can be obtained for power-law traps without making a high-η approximation [10]. These are exact within the truncated Boltzmann distribution approximation, and our numerical results agree with them exactly. In the high-η regime, simple analytic expressions can be found by making a high-η approximation [9, 20]. We find excellent agreement between our numerical calculations and these analytic expressions within their regime of validity.

The statistical mechanical quantities vary with temperature and ODT laser intensity, so integrals are evaluated at a dense series of temperature and laser intensity points. The variation with temperature and laser intensity is used to find interpolating functions for the temperature and laser intensity dependence of all quantities, which can then be used in place of time-intensive integral evaluations. Additionally, for time-dependent traps, lookup tables of trap depth and geometric average of the angular oscillator frequencies, which are the functions of ODT laser intensity, are necessary. It is important to note that the variation of U and all quantities calculated from U with ODT laser intensity allows us to model forced evaporation, since the ODT laser intensity is varied in a known way with time during the evaporation trajectory.

Using the interpolating functions, the atom number and temperature evolution can easily be found for a given initial condition from Eqs. 24 and 25 using an ordinary differential equations (ODE) solver in $Mathematica^{TM}$. All terms are either constants or functions of number and temperature and the independent variable time. This includes the total energy, E, so the ODE solver solves for $N(t)$ and $T(t)$ for the particular initial conditions and experimental parameters. Typically, one day is needed to create all lookup tables. After this preparation, a complete ODE solution for tens of seconds of sample evolution only requires a few seconds of computer evaluation time. The programs used for these simulations are available upon request.

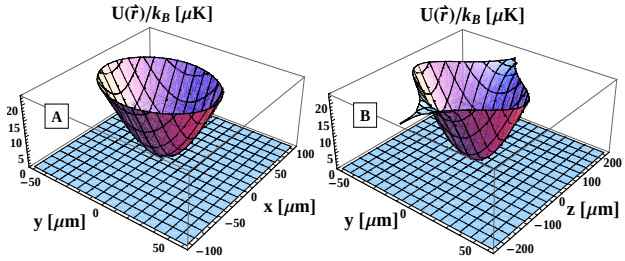

FIG. 3: (Color online) (A) The x-y cut and (B) the y-z cut of the ODT potential for approximately 9 W per beam. The boundary of the trap is the set of points with potential energy equal to the lowest saddle point, which is along the z axis. Gravity is oriented in the -$\hat{\mathbf{y}}$ direction. The beam nearly parallel to the x axis is slightly weaker and less focused than the beam along z, leading to the observed asymmetry.

V. EVAPORATION OF ^{88}SR AND ^{84}SR

Figure 4 shows the number and temperature of atoms as functions of time for ^{88}Sr $^1S_0$ atoms in the ODT with a constant potential. Various quantities such as the one-body loss rate, two-body inelastic collision rate constant, and elastic cross section can be determined by fitting the calculated evolution curves to experimental data. Three-body inelastic collisional loss is negligible here due to the extremely small three-body loss-rate constant L of ^{88}Sr [37].

We exclude the first second from the fit because we expect that atoms are far from equilibrium and significant population is still trapped in the individual beams of the ODT and not in the crossed region at this time. For this fit, we obtain the one-body loss rate $\Gamma_1 = 0.04\,\mathrm{s}^{-1}$, the ODT photon scattering rate $\Gamma_{ODT} = 0.03\,\mathrm{s}^{-1}$, and the s-wave scattering length of ^{88}Sr a_{88} to an uncertainty of $\pm\,0.4\,a_0$ (Fig. 4), but uncertainty in trap waists of $\pm\,5\,\mu$m increases the uncertainty of a_{88}, and we quote a final value of $a_{88} = 5.4\,^{+0.8}_{-0.6}\,a_0$ (the elastic scattering cross section $\sigma_{el}^{88} = 730^{+230}_{-150}\,a_0^2$), which matches what is predicted by theory based on photoassociative spectroscopy data [21]. Note that at the temperature of the sample studied here, σ_{el} differs significantly from its zero-temperature value, but sample temperature variation is small enough that the approximation of a constant cross-section during the simulation can describe the data well. (Appendix A describes how the energy dependence of the cross section is accounted for when comparing σ_{el} determined from this analysis with theory.) A good fit is found with $\beta_{in} = 0$ as expected since there are essentially no inelastic two-body loss processes in this system.

Figure 5 shows the simulation and data for ^{84}Sr $^1S_0$ atoms in a time-dependent trap. The power of ODT beams is ramped down according to $P = P_0/(1 + t/\tau)^\beta$, with time denoted by t, $\beta = 1.5$, and $\tau = 2\,s$, and the trap depth is reduced from 36 μK initially to 5 μK within 3.1 s. The peak phase space density during this interval is about 0.06, so

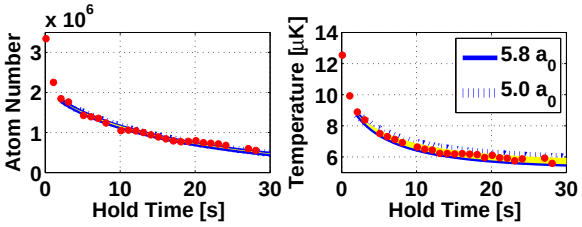

FIG. 4: (Color online) Variation of atom temperature and number with time for ^{88}Sr atoms in the $^1S_0$ state in a constant potential with a trap depth of 36 μK. The solid curve shows the fitting result for the upper bound of the s-wave scattering length of ^{88}Sr $a_{88} = 5.8\,a_0$, while the dashed one shows that for the lower bound of $a_{88} = 5.0\,a_0$.

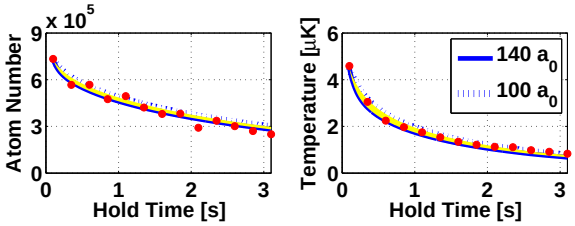

FIG. 5: (Color online) Variation of atom temperature and number with time for ^{84}Sr atoms in the $^1S_0$ state in a time-dependent trap. The solid curve shows the fitting result for the upper bound of the s-wave scattering length of ^{84}Sr $a_{84} = 140\,a_0$, while the dashed one shows that for the lower bound of $a_{84} = 100\,a_0$.

effects of quantum degeneracy can be neglected.

The s-wave scattering length of ^{84}Sr is $a_{84} = 122.7(3)\,a_0$ [21], so evaporation is much more efficient than for ^{88}Sr. Due to the large scattering length, three-body loss also becomes important. In this fit, we assume a value of the three-body loss-rate constant, $L^{84} = 3 \times 10^{-27}$ cm^6/s, which is found from the measured value for ^{86}Sr [38] and the a^4-scattering-length dependance of L [39]. The fit determines a_{84} to an uncertainty of $\pm\,20\,a_0$ (Fig. 5), but uncertainty in trap waists of $\pm\,5\,\mu$m increases the uncertainty of a_{84}, and we quote a final value of $a_{84} = 120\,^{+30}_{-40}\,a_0$, which is in good agreement with previous determinations [21, 40]. We are relatively insensitive to the values of Γ_1 and Γ_{ODT} because the sample evolution is fast, so we set these parameters to values implied by ^{88}Sr data. The agreement with the experimental value of a_{84} confirms the validity of the model for time-dependent traps, which was valuable for guiding recent experiments attaining quantum degeneracy in Sr [22, 25].

VI. CONCLUSION

In this paper, we have presented a model describing inelastic and elastic collision dynamics of trapped atoms that can treat traps lacking spatial symmetry and samples with a wide range of η, especially in low-η conditions. The main assumptions are ergodicity and a truncated Boltzmann velocity distribution. The model was used to describe ^{88}Sr and ^{84}Sr in an asymmetric ODT with low η and high η respectively, and collisional parameters extracted from the data were found to agree well with those from previous works. This model has been used to extract elastic and inelastic cross sections from experiments with metastable Sr atoms in an optical dipole trap [24] and to guide achievement of quantum degeneracy [22, 25].

Appendix A: Energy Dependence of the ^{88}Sr Elastic Collision Cross Section

Evaporation with an energy-dependent elastic collision cross section has been modeled in [12, 19], but these treatments assume a large cross section that varies because of the unitarity limit. In ^{88}Sr, the cross section varies because the scattering length is very small, as shown in Fig. 6 [21]. This variation is significant at microkelvin energies, which complicates comparison of theory and experiment because a distribution of collision energies contributes in a thermal sample in the ODT. A full energy-dependent kinetic calculation is beyond the scope of this model. We treat the variation in approximate fashion by assuming the system can be described by an effective, temperature-dependent cross section, $\langle\sigma_{el}\rangle$, that is an average of the collision-energy dependent cross section.

To relate $\langle\sigma_{el}\rangle$ to the underlying energy-dependent cross section, first consider the number of elastic collisions per second per unit volume at position $\mathbf{r}$ [41, 42]

$$Z(\mathbf{r}) = \frac{1}{2}\int d^3p_1 \int d^3p_2 \sigma_{el} |\mathbf{v_1} - \mathbf{v_2}| f(\mathbf{r}, \mathbf{p_1}, t) f(\mathbf{r}, \mathbf{p_2}, t), \tag{A1}$$

where $\mathbf{v_1} = \mathbf{p_1}/m$, $\mathbf{v_2} = \mathbf{p_2}/m$. For the ultracold regime, $\sigma_{el}(E_{coll})$ can only depend on the collision energy $E_{coll} = p^2/2\mu$ for $p = \mu\,|\mathbf{v}_1 - \mathbf{v}_2|$ and the reduced mass $\mu = m/2$. The average cross-section will not depend on density, so we can assume a constant density. For simplicity, we use untruncated Maxwell-Boltzmann distributions for f, which yields

$$Z = \frac{2\pi n_0^2}{\mu}\int dp\, p^3 \frac{\sigma_{el}(E_{coll})}{(2\pi\mu k_B T)^{3/2}} e^{-\frac{p^2}{2\mu k_B T}}. \tag{A2}$$

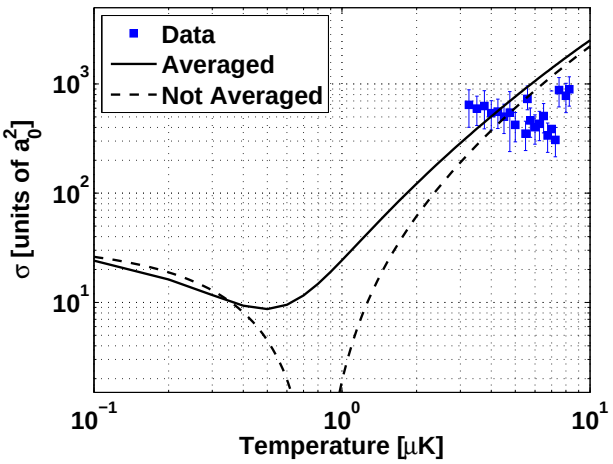

FIG. 6: Measurements and theories for the ^{88}Sr elastic collision cross section, σ_{el}. The dashed curve is the energy-dependent elastic collision cross section [21] for a collision energy of $E_{coll} = 2k_BT$, which is an average collision energy as described in the text. The solid line is an average cross section, weighted by the rate of collisions of a given energy, for the temperature T.

For an energy-independent cross section, this would reduce to the standard result [41]

$$Z = 2\sigma_{el} n_0^2 \sqrt{\frac{k_B T}{\pi m}}. \tag{A3}$$

For a given sample temperature, there is a distribution of collision energies, and if the cross section is energy dependent, this would imply a distribution of cross sections. We treat this possibility, which is important for ^{88}Sr collisions, by calculating an effective cross section, $\langle\sigma_{el}\rangle$, that can be used in our simulations. This quantity is an average of the true cross section over energy, and in principle it can vary with temperature.

To arrive at a value for $\langle\sigma_{el}\rangle$ from the theoretical $\sigma_{el}(E_{coll})$ for ^{88}Sr [21] we assume that the evaporation rate can be described by an average of $\sigma_{el}(E_{coll})$ in which the weighting is proportional to the contribution of each collision energy to the total number of collisions per time in the sample. (Using this weighting, the average collision energy for a given temperature T for an energy-independent cross section is $2k_BT$.) For a given equilibrium temperature, this average cross section is given by

$$\langle\sigma_{el}\rangle = \frac{Z}{2n_0^2\sqrt{\frac{k_BT}{\pi m}}}, \tag{A4}$$

where Z is calculated numerically using Eq. A2 and the energy dependence of σ_{el} that was determined from photoassociation data [21]. Contribution to Z is not exactly equivalent to contribution to the evaporation rate, but this is a reasonable approximation in the spirit of [12].

Figure 6 shows variation of $\sigma_{el}(E_{coll})$ and $\langle\sigma_{el}\rangle$ for ^{88}Sr as well as experimental data in which the numerical model is used to determine the best-fit σ_{el} in Eq. 25. The reasonable match of theory and experiment gives confidence in the numerical model in the low-η regime. Error bars represent statistical variation. In addition, there is systematic uncertainty due to uncertainty in the trapping potential of typically a factor of two, but this becomes more of an issue for lower sample temperatures and shallower traps, which are more challenging to characterize and model due to the importance of gravity. The assumption of ergodicity may also be less valid at lower temperature because the elastic collision rate and η become very small.

ACKNOWLEDGMENTS

We thank P. Julienne, R. Côté, and P. Pelligrini for helpful discussions and D. Comparat for sharing the original code for describing collisional dynamics of trapped atoms at high η. This work was supported by the Welch Foundation

(C-1579), National Science Foundation (PHY-0855642), and the Keck Foundation.

[1] H. F. Hess, Phys. Rev. B **34**, 3476 (1986).
[2] T. J. Tommila, Europhys. Lett. **2**, 789 (1986).
[3] F. Dalfovo, S. Giorgini, L. P. Pitaevskii, and S. Stringari, Rev. Mod. Phys. **71**, 463 (1999).
[4] S. Giorgini, L. Pitaevskii, and S. Stringari, Rev. Mod. Phys. **80**, 1215 (2008).
[5] E. A. Burt, R. W. Ghrist, C. J. Myatt, M. J. Holland, E. A. Cornell, and C. E. Wieman, Phys. Rev. Lett. **79**, 337 (1997).
[6] K. M. Jones, E. Tiesinga, P. D. Lett, and P. S. Julienne, Rev. of Mod. Phys. **78**, 483 (2006).
[7] R. V. Krems, Int. Rev. Phys. Chem. **24**, 99 (2005).
[8] K. B. Davis, M.-O. Mewes, and W. Ketterle, Appl. Phys. B **60**, 155 (1995).
[9] W. Ketterle and N. J. van Druten, Adv. Atom. Mol. Opt. Phys. **37**, 181 (1996).
[10] O. J. Luiten, M. W. Reynolds, and J. T. M. Walraven, Phys. Rev. A **53**, 381 (1996).
[11] K. Berg-Sørensen, Phys. Rev. A **55**, 1281 (1997).
[12] P. J. J. Tol, W. Hogervorst, and W. Vassen, Phys. Rev. A **70**, 013404 (2004).
[13] M. J. Holland, B. DeMarco, and D. S. Jin, Phys. Rev. A **61**, 053610 (2000).
[14] C. A. Sackett, C. C. Bradley, and R. G. Hulet, Phys. Rev. A **55**, 3797 (1997).
[15] K. M. O'Hara, M. E. Gehm, S. R. Granade, and J. E. Thomas, Phys. Rev. A **64**, 051403(R) (2001).
[16] H. Wu and C. J. Foot, J. Phys. B **29**, L321 (1996).
[17] Z. Y. Ma, A. M. Thomas, C. J. Foot, and S. L. Cornish, J. Phys. B **36**, 3533 (2003).
[18] R. Grimm, M. Weidemüller, and Y. B. Ovchinnikov, Adv. Atom. Mol. Opt. Phys. **42**, 95 (2000).
[19] D. Comparat, A. Fioretti, G. Stern, E. Dimova, B. L. Tolra, and P. Pillet, Phys. Rev. A **73**, 043410 (2006).
[20] R. deCarvalho and J. Doyle, Phys. Rev. A **70**, 053409 (2004).
[21] Y. N. Martinez de Escobar, P. G. Mickelson, P. Pellegrini, S. B. Nagel, A. Traverso, M. Yan, R. Côté, and T. C. Killian, Phys. Rev. A **78**, 062708 (2008).
[22] Y. N. Martinez de Escobar, P. G. Mickelson, M. Yan, B. J. DeSalvo, S. B. Nagel, and T. C. Killian, Phys. Rev. Lett. **103**, 200402 (2009).
[23] S. Stellmer, M. K. Tey, B. Huang, R. Grimm, and F. Schreck, Phys. Rev. Lett. **103**, 200401 (2009).
[24] A. Traverso, R. Chakraborty, Y. N. Martinez de Escobar, P. G. Mickelson, S. B. Nagel, M. Yan, and T. C. Killian, Phys. Rev. A **79**, 060702(R) (2009).
[25] P. G. Mickelson, Y. N. Martinez de Escobar, M. Yan, B. J. DeSalvo, and T. C. Killian, Phys. Rev. A **81**, 051601(R) (2010).
[26] B. J. DeSalvo, M. Yan, P. G. Mickelson, Y. N. Martinez de Escobar, and T. C. Killian, Phys. Rev. Lett. **105**, 030402 (2010).
[27] S. B. Nagel, C. E. Simien, S. Laha, P. Gupta, V. S. Ashoka, and T. C. Killian, Phys. Rev. A **67**, 011401(R) (2003).
[28] S. B. Nagel, P. G. Mickelson, A. D. Saenz, Y. N. Martinez, Y. C. Chen, T. C. Killian, P. Pellegrini, and R. Côté, Phys. Rev. Lett. **94**, 083004 (2005).
[29] P. G. Mickelson, Y. N. Martinez, A. D. Saenz, S. B. Nagel, Y. C. Chen, T. C. Killian, P. Pellegrini, and R. Cote, Phys. Rev. Lett. **95**, 223002 (2005).
[30] P. G. Mickelson, Y. N. Martinez de Escobar, P. Anzel, B. J. DeSalvo, S. B. Nagel, A. J. Traverso, M. Yan, and T. C. Killian, J. Phys. B **42**, 235001 (2009).
[31] H. Katori, T. Ido, Y. Isoya, and M. Kuwata-Gonokami, Phys. Rev. Lett. **82**, 1116 (1999).
[32] J. Ye, H. J. Kimble, and H. Katori, Science **320**, 1734 (2008).
[33] S. Friebel, C. D'Andrea, J. Walz, M. Weitz, and T. W. Hänsch, Phys. Rev. A **57**, R20 (1998).
[34] W. D. Phillips, in *Proceedings of the International School of Physics Enrico Fermi; course 118, Laser Manipulation of Atoms and Ions*, edited by E. Arimondo, W. Phillips, and F. Strumia (North-Holland, New York, 1992), p. 289.
[35] C.-L. Hung, X. Zhang, N. Gemelke, and C. Chin, Phys. Rev. A **78**, 011604 (2008).
[36] M. Yan, Master's thesis, Rice University (2011).
[37] G. Ferrari, R. E. Drullinger, N. Poli, F. Sorrentino, and G. M. Tino, Phys. Rev. A **73**, 023408 (2006).
[38] S. Stellmer, M. K. Tey, R. Grimm, and F. Schreck, Phys. Rev. A **82**, 041602 (2010).
[39] B. D. Esry, C. H. Greene, and J. P. Burke, Phys. Rev. Lett. **83**, 1751 (1999).
[40] A. Stein, H. Knöckel, and E. Tiemann, Eur. Phys. J. D **57**, 171 (2010).
[41] K. Huang, *Statistical Mechanics* (Wiley, New York, 1987).
[42] D. A. McQuarrie, *Statistical Mechanics* (University Science Books, Sausalito, 2000).